Mechanisms of Ultrashort Laser-Induced Fragmentation of Metal Nanoparticles in Liquids: Numerical Insights

ARTICLE *in* THE JOURNAL OF PHYSICAL CHEMISTRY C · JUNE 2015

Impact Factor: 4.77 · DOI: 10.1021/acs.jpcc.5b02084

2 AUTHORS, INCLUDING:

Tatiana Itina
French National Centre for Scientific Research
187 PUBLICATIONS **1,685** CITATIONS

THE JOURNAL OF PHYSICAL CHEMISTRY C

Article

pubs.acs.org/JPCC

Mechanisms of Ultrashort Laser-Induced Fragmentation of Metal Nanoparticles in Liquids: Numerical Insights

Laure Delfour and Tatiana E. Itina*

Laboratoire Hubert Curien, UMR CNRS 5516/Université de Lyon, Bât. F, 18 rue du Prof. Benoit Lauras, 42000 Saint-Etienne, France

ABSTRACT: Femtosecond laser-induced fragmentation of gold nanoparticles in water is examined. Numerical calculations are performed to elucidate the roles of thermal and electrostatic effects due to electron emission in the corresponding decomposition mechanisms. The obtained results demonstrate that particles smaller than a well-defined size R^* melt at smaller fluences than the ones required for electrostatic decomposition. The limiting size depends on the absorption coefficient calculated as a function of particle radius, which depends on laser wavelength and on the optical properties of the particle and the background environment. To decompose particles with radii larger than R^*, a considerable increase in laser fluence is required. In this case, thermomechanical effects become prevailing. Both the calculated range of particle sizes to be decomposed by the considered laser pulses and the corresponding fluences agree with several experimental measurements.

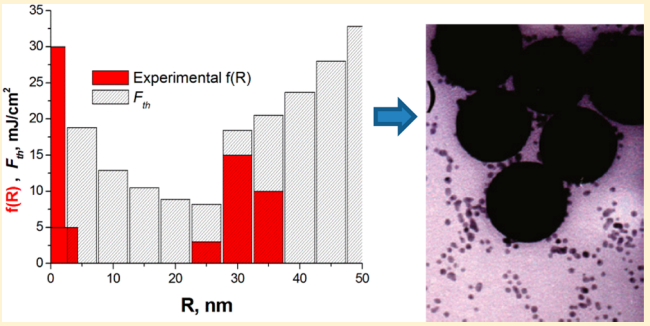

INTRODUCTION

During the past decade, nanoparticles (NPs) have found numerous applications in different areas. Thus, metallic NPs are now widely used in photonics, electronics, chemistry, medicine, textile production, and sensors for chemistry and biology.[1−7] A promising recently emerging field of NP application concerns new energy sources. For the development of this application, fusion dynamics in laser−cluster interactions was investigated, with a hope to obtain high neutron yields of about 10 keV−15 MeV.[8−10] Laser−particle interactions are key processes in this case, as well as in the case of cancer treatment[9−16] and sensor and quantum dot development.[17] The unique plasmonic properties of the metallic NPs make them particularly suitable for these applications. In addition, laser-based fragmentation of nanoparticles is found to be a promissing method of control over nanoparticle size distribution.

In particular, a constantly growing number of modern applications are based on short (picosecond) and ultrashort (femtosecond) laser interactions with metal NPs. Such laser pulses induce a temperature rise both in the particle and around it, triggering several effects.[18,19] The first one is a trivial thermal expansion of the particle, when acoustic waves are launched. Then, in the presence of an ambient liquid, a microbubble can be formed following the shock wave generation if laser fluence is sufficiently high.[20,21] Particle temperature can reach the melting or boiling point, leading to thermal evaporation and/or decomposition. These processes are typically combined with mechanical and electrostatic effects that can also account for particle fragmentation.[11] Furthermore, intense ultrashort laser interactions with small clusters are known to induce Coulomb explosion in vacuum.[22] In fact, because the electron subsystem is heated first, electrons can be removed, leaving positively charged ions that are subjected to a repulsive force. In this scenario, clusters explode, ejecting energetic ions. For larger particles, furthermore, Mie theory provides a strongly non-homogeneous field distribution, leading to a preferential mass removal at the poles of the particle due to the near-field ablation.[23] These previous investigations demonstrated that particle can be fragmented either due to thermomechanical effects or due to electron emission followed by Coulomb explosion. The prevailing effect depends both on particle parameters, such as size and material, and on laser-related parameters, such as fluence, wavelength, and pulse duration. The role of these effects is still under discussion.

Herein, we present the results of a computational study aimed at a better understanding of the underlying physical processes involved in laser−NP interactions. In particular, our objective is definition of the role of both particle and laser parameters in the major particle fragmentation mechanisms. The corresponding thresholds are calculated and compared with the available experimental findings. In addition, we perform molecular dynamics (MD) simulations to visualize the particle time evolution in the absence of Coulomb explosion. The first part contains modeling details, while the second part is devoted to the analysis of the obtained results.

Received: March 3, 2015
Revised: May 25, 2015

DOI: 10.1021/acs.jpcc.5b02084
J. Phys. Chem. C XXXX, XXX, XXX−XXX

MODELING DETAILS

In this study, we consider ultrashort laser interactions with metal nanoparticles at rather moderate laser fluences, below the ones used in laser fusion experiments. In this case, laser energy is first absorbed by the conduction electrons. The energy is then transferred to the lattice through electron−lattice coupling. Finally, energy exchange transfers it to the surrounding medium, if any, where it diffuses. Because femtosecond pulse duration is much shorter than the electron−phonon relaxation time, electronic temperature rises very quickly up to several thousand kelvins, whereas lattice temperature stays close to room temperature during electron−lattice relaxation time. Consequently, we account for both electron and phonon subsystems separately by using a so-called "two-temperature model" or TTM.[24,25] Furthermore, if nanoparticles are placed in a liquid, an additional equation is added to account for the increase in medium temperature, resulting in a three-temperature model. The corresponding equation system is written as follows:[18,26]

$$\begin{cases} C_e(T_e)\dfrac{dT_e}{dt} = -G(T_e)(T_e - T_l) + S(t) \\ C_l(T_l)\dfrac{dT_l}{dt} = G(T_e)(T_e - T_l) - F \\ C_m(T_m)\dfrac{dT_m}{dt} = F \end{cases} \quad (1)$$

where the first equation describes the evolution of the electronic temperature T_e coupled to the lattice, and includes the energy exchange with the laser pulse. The second equation expresses the dynamics of the lattice temperature T_l, including heat transfer across the interface. C_e, C_l, and C_m are respectively the electron, lattice, and medium heat capacities. The dependencies of C_e and of the electron−phonon coupling constant G on electron temperature T_e were previously calculated for several metals based on their electron density of states (EDOS), with the effect of thermal excitation of the electrons (including d electrons) taken into account.[27,28] Heat diffusion is neglected here because we are interested only in very short time scales, on the order of picoseconds.[4] The corresponding values were experimentally measured for C_m.[29] For liquid phase, gold heat capacity is $C_l = 0.149\ J{\cdot}g^{-1}{\cdot}K^{-1}$, whereas we use the following expression for gold solid phase[30] with the same units:

$$C_l = 0.119 + (3.061 \times 10^{-5})T_l \quad (2)$$

The source term $S(t)$ that describes laser energy absorption is expressed by

$$S(t) = \frac{\sigma_{abs}(n_m, R)I(t)}{V(T_l)} \quad (3)$$

where σ_{abs} is the absorption cross section of the nanoparticle, $V(T_l)$ is the particle volume, $I(t)$ is the pulse intensity, and R is the nanoparticle radius. Gaussian time profile is assumed for the laser pulse with duration τ (full width at half-maximum of the Gaussian time profile) and laser fluence f. Furthermore, laser intensity $I(t)$, which is involved in the source term $S(t)$ in eq 1, is written as follows:

$$I(t) = \frac{2f\sqrt{\ln 2}}{\tau\sqrt{\pi}} e^{(-4t^2 \ln 2/\tau^2)} \quad (4)$$

In addition, particle thermal expansion is taken into account as a function of the lattice temperature T_l by calculating particle volume $V(T_l)$. Thus, particle radius R depends on the thermal expansion coefficient α of gold, which is calculated as[32] $\alpha = (3.724 \times 10^{-5}) + (15.236 \times 10^{-10})T_l$. The energy loss term F describes the heat exchange with the surrounding media and is described by

$$F = \frac{3h(T_l - T_m)}{R_{np}} \quad (5)$$

where the energy exchange coefficient h is 105.106 $W/m^2{\cdot}K$ for the gold−water interface.

Generally, light interactions with small particles strongly depend on particle size, shape, and material, as well as on the composition of the environment in which the particle is embedded. Here, for simplicity, particle shape is set to be spherical. Therefore, the absorption cross-section $\sigma_{abs}(R, \lambda, n_m)$ of the gold particles depends on laser wavelength λ and particle radius R (Figure 1a) and also on the refractive index n_m of the medium (Figure 1b). If particle size becomes comparable to laser wavelength, a red shift of the surface plasmon resonance appears. Moreover, the absorption cross section behavior at fixed particle radius depends on the refractive index value of the medium. For n_m = 1.33 (liquid water), surface plasmon resonance is more pronounced than for n_m = 1.00 (water vapor).

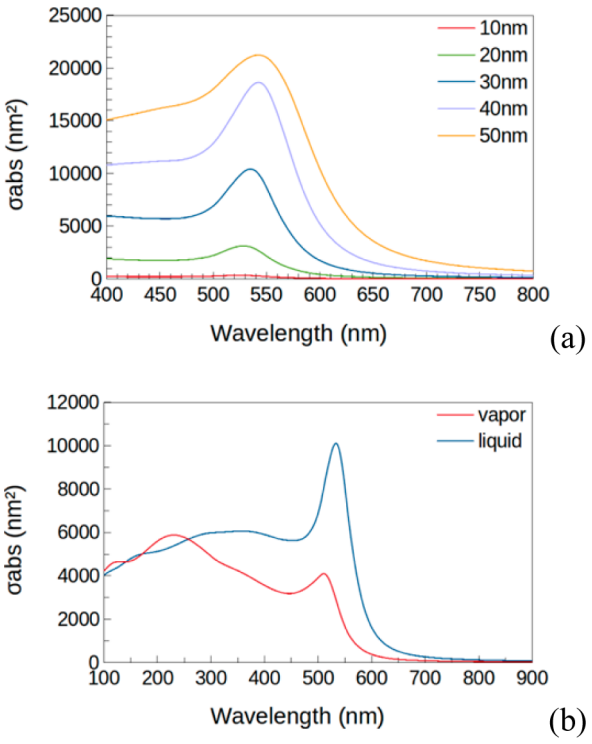

Figure 1. (a) Absorption cross section of a gold particle as a function of wavelength, for particle radius between 10 and 50 nm. (b) Absorption cross sections of a gold particle with 30 nm radius in water and in vapor phase.

The absorption cross section, σ_{abs}, is calculated by using Mie theory for a spherical gold particle.[32,33] To relate the cross section σ_{mie} to the physical cross section πR^2 of the particle, an efficiency factor Q_{mie} is used, so that $Q_{mie} = \sigma_{mie}/\pi R^2$. This procedure is used for extinction, scattering, and absorption

DOI: 10.1021/acs.jpcc.5b02084
J. Phys. Chem. C XXXX, XXX, XXX−XXX

coefficients (Q_{ext}, Q_{scat}, and Q_{abs}). The absorption coefficient strongly varies with particle radius when R < 80 nm (Figure 2a). In this dependency, a maximum is observed in the

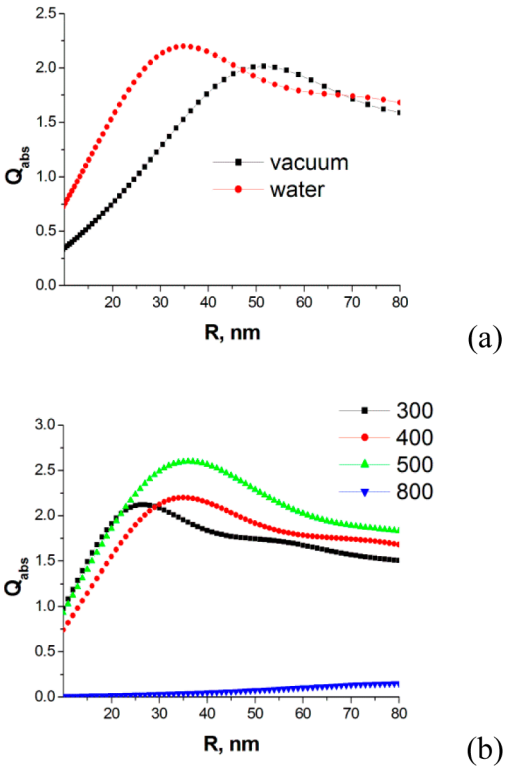

Figure 2. Absorption coefficient for gold NP as a function of particle radius: (a) in the presence of water and in vacuum for laser wavelength of 400 nm and (b) in water for different incident wavelengths.

calculated dependency for gold NP, where the corresponding R_m* value depends both on the surrounding medium (Figure 2a) and on laser wavelength (Figure 2b). Clearly, particle size strongly affects absorption. This effect is accounted for in the laser source term $S(t)$ in our TTM model (eq 1). Our model also accounts for the variation of refractive index as a function of wavelength for the background environment (here, water).[33]

Finally, the enthalpy consumption for gold ΔH is taken into account.[34,35] Thus, melting energy is calculated as follows

$$E_{ph} = \rho_{gold} V \Delta H \tag{6}$$

where ρ_{gold} = 19 300 kg/m^3 and $\Delta H = 1.212 \times 10^9$ J/m^3. If h is the previously defined thermal conductance and A is the particle area, then the energy exchange at the gold−water interface, Q, is

$$Q = Ah(T_l - T_m) \tag{7}$$

When the particle starts to melt and until it is completely melted, T_l remains constant. Complete melting is achieved when the following condition is satisfied:

$$\int_0^t [VG(T_e - T_l) - Q]\, dt = E_{ph} \tag{8}$$

Time evolutions of electron, lattice, and ambient temperature given by the model (eqs 1−8) agree quite well with previous calculation results of Werner et al.[18,19] thus confirming the model validity (Figure 3).

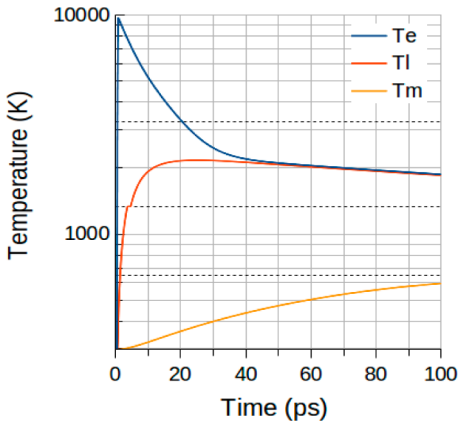

Figure 3. Calculated time evolution of electron, lattice, and water temperature for gold nanoparticle with radius of 30 nm in water. Here, laser temporal pulse width is 150 fs, wavelength is 400 nm, and laser fluence is 12.3 mJ/cm^2 (Gaussian time profile).

To check the possibility of the electrostatic mechanisms based on Coulomb explosion for the considered laser pulses, thermionic electron emission is considered as follows.[18,19,26,34] Based on the calculated electronic temperature of the particle, the total number of electrons ejected from the particle is given by

$$N_{therm} = \alpha n_\varepsilon \tag{9}$$

where α = 4 V/a_{fcc}^3 is the total number of atoms in the particle and a_{fcc} = 4.08 Å is the lattice constant of a face-centered cubic (fcc) unit cell for gold. n_ε is the number of electrons that exceed the work function per atom at the electron temperature T_e as follows:

$$n_\varepsilon = \int_\varepsilon^\infty \mathrm{EDOS}(E) f(E, \mu(T_e), T_e)\, dE \tag{10}$$

In this expression, $\varepsilon = E_F + w$, where w is the work function of gold and E_F is the Fermi energy of gold. Chemical potential $\mu(T_e)$ is calculated by density functional theory (DFT) methods.[30] In eq 10, typically EDOS is computed at T_e = 0 K, introducing a partial electronic temperature dependence on the Fermi−Dirac distribution of electrons only.[34] However, because EDOS is a function of the electronic temperature T_e, for comparison we also use here EDOS(T_e) functions for gold.[30] Gold work function w = 5.1 eV is based on the Fermi energy, E_F = 10.23 eV.

When metal NPs are irradiated by ultrashort laser pulses, their electrons are first heated well before the lattice temperature. Thus, part of the electrons can be ejected, leaving behind a positively charged particle. If the remaining charge is high enough, the repulsive Coulomb forces may overcome the attractive cohesive forces. When the energy of the electron subsystem is above E_F and is high enough for a sufficient number of electrons to be thermally ejected, the nanoparticle cannot remain stable. This phenomenon is typically described by a so-called "liquid drop" model using a Rayleigh instability factor:

$$X = \left(\frac{N_{therm}^2}{N_e}\right) \Big/ \left(\frac{16\pi r_{ws}^3 \sigma_s}{e^2}\right) \tag{11}$$

Here N_{therm} is the total number of emitted electrons, r_{ws} is the Wigner−Seitz radius, and e is the elementary electric charge.

DOI: 10.1021/acs.jpcc.5b02084
J. Phys. Chem. C XXXX, XXX, XXX−XXX

Each gold atom is supposed to have one valence electron, thus the total number of free electrons N_e equals α. The surface tension σ_s is 8.78 N/m for the solid phase, whereas the temperature dependence for the liquid phase[36] is given by

$$\sigma_s = 1.15 + (0.14 \times 10^{-3})(T_l - T_m) \quad (12)$$

For liquid gold, the instability factor reduces to $X = 0.9(N_{therm}^2/a_{fcc})$. In vacuum, typically, thermal effects take place[18] for X values smaller than 0.3. Otherwise, according to the liquid drop model, the particle should fragment due to electrostatic repulsion. For values of X between 0.3 and 1, particle fission was shown to occur[18] together with thermal evaporation.[35−37] If a sufficient number of electrons is ejected, an instability is known to develop due to the growing positive charge. It was noted,[19] however, that melting should occur first for the liquid drop model to be applicable. If laser interaction takes place in a liquid, furthermore, electron and particle solvation should not be negligible. These effects may considerably diminish the probability of Coulomb explosion in water.

RESULTS AND DISCUSSION

In this section, we present calculation results obtained for gold nanoparticles in water absorbing a Gaussian laser pulse of 150 fs at 400 nm. These laser parameters are similar to the experimental conditions considered by Werner et al.[18,19]

First, we check at what electron temperatures electrostatic decomposition should occur. The calculations performed for a gold particle with R = 30 nm show that to reach X = 0.3 the electron subsystem should be heated at least up to $T_e \approx 8030$ K in the calculations with T_e-independent EDOS. This value is only slightly larger, $T_e \approx 8150$ K, when T_e-dependent EDOS is used (Figure 4). The obtained results agree with previous findings of Hashimoto et al.[38]

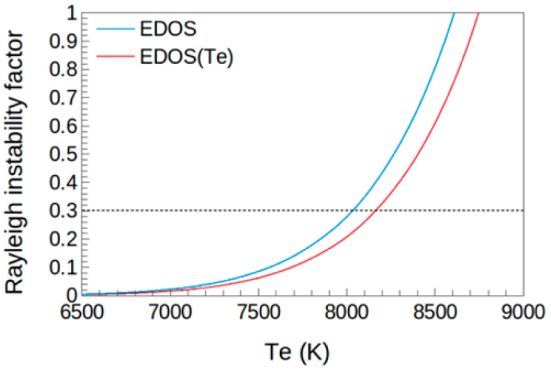

Figure 4. Rayleigh instability factor as a function of electronic temperature obtained by use of constant EDOS (blue) and for T_e-dependent EDOS (red).

Then, we consider gold NPs with various sizes in the range of radius R between 5 and 70 nm. For this, a series of calculations are performed for 400 nm laser wavelength by varying laser fluence. We correlate the absorbed fluence with that required for melting, boiling, and Coulomb explosion of nanoparticles with different radii (Figure 5a). One can see in the figure that well-defined minima are observed in the threshold curves that can be explained by the maximum revealed in the absorption coefficient. Evidently, the absorbed laser fluence[35] strongly depends on the absorption coefficient; see Figure 2a.

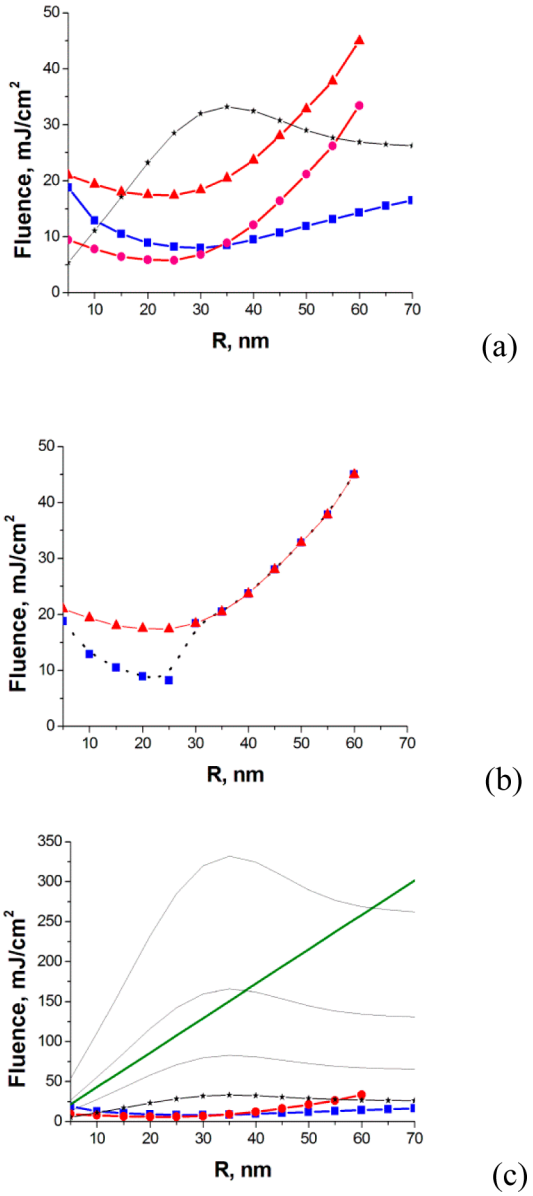

Figure 5. (a) Laser fluences as a function of particle radius: absorbed fluence obtained at incident fluence of $f_0 \approx 12.3$ mJ/cm^2 (black) and laser fluence needed for melting (magenta), for reaching boiling temperature (red), and for electrostatic decomposition (blue). (b) Calculated fragmentation fluence threshold as a function of particle radius. (c) Fluence corresponding to particle cohesive energy (green) and calculated absorbed fluence obtained at incident fluence of f_0 (black line with symbols), $2.5f_0$, $5f_0$, and $10f_0$ (black lines).

Interestingly, an intersection of the melting curve with the curve corresponding to Coulomb explosion is observed at around $R^* \approx 30$ nm, showing the validity limits of the liquid drop model. These curves also show a range of particle sizes that can be decomposed at a given incident fluence. For instance, the applied 400 nm and 150 fs laser pulses are efficient in decomposition of particles with radius from 10 nm to R^*. For this particle size range, the melting threshold is smaller than the minimum laser fluence required for Coulomb explosion. As a result, these particles are expected to decompose by the mechanism given by the liquid drop model (part of the blue curve for R between 5 and ~30 nm). To decompose larger particles, one should increase laser

DOI: 10.1021/acs.jpcc.5b02084
J. Phys. Chem. C XXXX, XXX, XXX−XXX

fluence strongly above 10 J/cm^2, as was shown by Werner et al.[18,19]

For particles larger than R^*, melting threshold is larger than the one given by the liquid drop model for Coulomb explosion. In addition, the minimum in the Coulomb explosion threshold corresponds to $R^* \approx 30$ nm, the population that was shown to survive in the experiments of Werner et al. at the considered laser parameters. Thus, it can be suggested that these particles mostly evaporate, so that the resulting threshold is much higher and is given by the corresponding part of the boiling curve. The resulting threshold is shown in Figure 5b as a function of particle radius.

In addition, Figure 5b shows that, at the given laser pulse parameters, only particles with a particular size range are subjected to size reduction. For instance, at 12.3 mJ/cm^2 at 400 nm and 150 fs, only particles with R from 10 to 30 nm are expected to be decomposed. To evaporate particles with radius ~30 nm and larger by the same laser pulse, one should increase laser fluence above ~10−20 mJ/cm^2. The obtained fragmentation fluence can explain the formation of a bimodal size distribution,[19] typically observed in multipulse laser experiments with metallic nanoparticles in liquids.

It is instructive to compare the calculated size reduction thresholds with laser fluence required to overcome gold cohesive energy, ~3.81 eV/atom (Figure 5c). One can see that, to absorb such energy per atom at the considered laser wavelength and pulse duration, the incident laser fluence should be much above f_0. For instance, the required incident fluence should be as high as ~170 mJ/cm^2 for $R < 40$ nm to this effect in the absence of the Coulomb explosion. We note that this value is much higher than the experimentally used ones.[18]

Figure 6 reveals good correlation of the obtained decomposition threshold curve with the experimentally observed particle populations.[19] Similar populations were obtained in these experiments starting from an initial ensemble of nanoparticles with diameter around 60 nm with dispersion ~10 nm by using multipulse irradiation at 400 nm and 150 fs

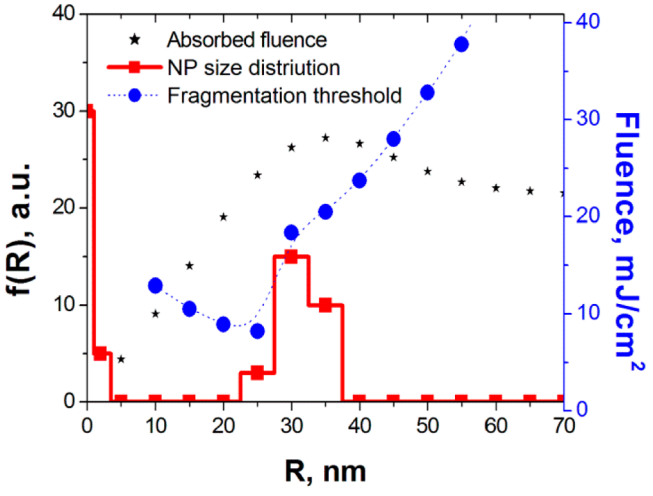

Figure 6. (Red histogram) Typical nanoparticle populations observed in experiments[18,19] with multipulse irradiation; (blue spheres) calculated decomposition threshold as a function of particle radius for 400 nm and 150 fs laser pulse; and (black stars) absorbed laser fluence as a function of particle radius for incident fluence of 12.3 mJ/cm^2 at 400 nm and 150 fs laser pulse.

below ~10 J/cm^2 at both 100 Hz and at 1 kHz at laser fluence. Interestingly, particles with radius $R \approx 30$−35 nm remained practically unaffected by laser pulses. One can see in the figure that the sharp increase in the calculated decomposition threshold well correlates with the remaining population. These results confirm the validity of the presented model. Only when laser fluence was >10 J/cm^2 at 1 kHz was the population initially centered on $R \approx 30$ nm shifted to smaller sizes ($R \approx 17$ nm) in the experiments. This result was attributed to possible cumulative effects, which require more investigation.

Finally, molecular dynamics simulations are performed for a spherical gold particle with the radius of 15 nm in vacuum. Here, LAMMPS code and EAM potential (Au_u3.eam)[39] are used. The nanoparticle is first quenched to form a surface and is heated to room temperature. After that, energy is given to the particle atoms, as it would be received from the electron subsystem, by following the lattice temperature evolution obtained from the TTM model for 150 fs and laser wavelength is 400 nm.

Figure 7 shows an example of lattice temperature time evolution calculated for 30 mJ/cm^2. In detail, particle heating is

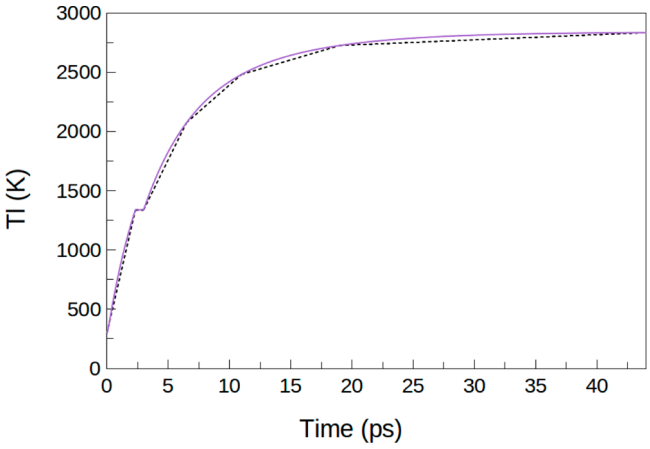

Figure 7. Typical time evolution of the lattice temperature. The solid line corresponds to results from the TTM calculations for gold particle with R = 15 nm, where laser wavelength is 400 nm, temporal pulse width is 150 fs, and laser fluence is 30 mJ/cm^2. The dashed line shows the fit used in MD calculations.

simulated by using linear fits to the calculated curve $T_l(t)$ through temperature rescaling by applying LAMMPS NVE procedure to a 50 × 50 × 50 nm unit box containing the nanoparticle placed in its center until ~45 ps. After that, the system is allowed to evolve without temperature control. Electron dynamics and related processes are disregarded in these simulations, so that these results show what would happen if only thermomechanical effects occur.

Figure 8 shows calculation results obtained for R = 15 nm at laser fluence as high as 30 mJ/cm^2. Here, in the absence of the electrostatic effects, this result should be analyzed on the basis of the the cohesive threshold, as shown in Figure 5c. We note that in vacuum the absorption coefficient is smaller than in water (Figure 2a). One can see that the nanoparticle starts to expand and a void appears in its center at 30 ps (Figure 7b), which continues to grow until 109 ps (Figure 8c−e). In addition to purely thermal effects and surface tension, the

DOI: 10.1021/acs.jpcc.5b02084
J. Phys. Chem. C XXXX, XXX, XXX−XXX

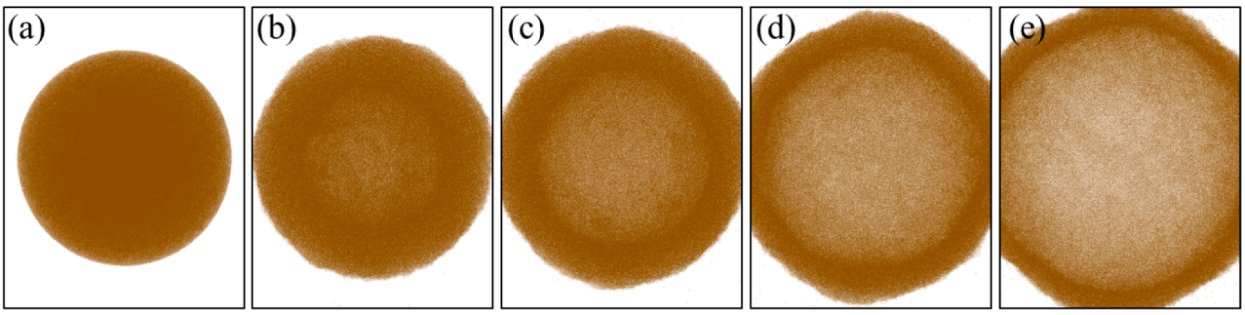

Figure 8. Nanoparticle shape evolution for gold nanoparticle with radius of 15 nm in vacuum, calculated for laser wavelength of 400 nm, pulse duration of 150 fs, and fluence of 30 mJ/cm^2. Obtained results are shown at time delays of (a) 11.6, (b) 30, (c) 43.75, (d) 66, and (e) 109 ps after the beginning of the laser pulse.

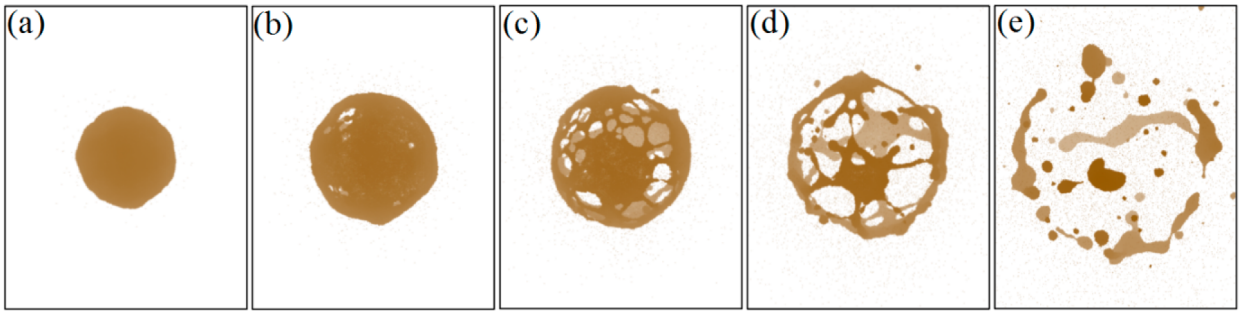

Figure 9. Nanoparticle shape evolution for gold nanoparticle with radius of 15 nm in vacuum calculated for wavelength of 400 nm, pulse duration of 150 fs, and fluence of 100 mJ/cm^2. Obtained results are shown at time delays of (a) 46, (b) 86.5, (c) 119.5, (d) 165, and (e) 281 ps after the beginning of the laser pulse.

effects of internal pressure wave and stress confinement play a role here.[40]

In the performed molecular dynamics calculations, only particle reshaping is observed at laser fluences smaller than ∼27 mJ/cm^2. Figure 9 demonstrates what happens if a much higher laser fluence is applied. In this case, the particle is heated very rapidly, so that pressure grows up very quickly to the point where the particle is suddenly fragmented into many small chunks.[42,43] Figure 9b shows that this effect begins appearing at 86.5 ps, whereas Figure 9e shows the sizes of these fragments.

The results of these presented simplified molecular dynamics simulations can be considered as another indication that, for particles with $R < 30$ nm, electron dynamics and electrostatic effects should be taken into account; otherwise laser-induced fragmentation would require a considerable increase in laser fluence. For larger particles, however, thermal evaporation explains fairly well the available experimental findings,[18,19] as Figure 6 demonstrates. Thus, our results confirm the previously underlined role of the Coulomb explosion[41] only for rather small particles and agree with the predicted role of thermal effects[34] for larger particles.

CONCLUSIONS

We have presented the results of a numerical investigation of femtosecond laser-induced particle fragmentation. For this, first we have developed a thermal model that has been combined with one for electron emission.

The performed analysis of the numerical results clearly demonstrates that there is a maximum in size dependence of the absorption fluence that is shifted to larger sizes when laser wavelength increases. This maximum depends also on the optical properties of both particle material and background environment. For gold in water at 400 nm, it is located around $R^* \approx 30$ nm. This result depends on the absorption coefficient and strongly affects energy source in the presented two-temperature model.

Then, we have performed a series of calculations in order to determine both thermal and electrostatic decomposition thresholds. For this, laser fluence required to reach melting, boiling, and Coulomb explosion have been calculated as a function of particle sizes. The intersections of melting curves with absorption curves were determined, and the required absorbed laser fluences were obtained.

As a result of comparison of different mechanisms, a well-defined minimum in the threshold curve around R^* is predicted, below which electrostatic explosion is possible, whereas thermomechanical explosion is expected for larger particles at more than twice larger laser fluences. These results correlate well with previous experiments and can be used to predict fragmentation probability of gold nanoparticles by ultrashort laser pulses.

AUTHOR INFORMATION

Corresponding Author

*E-mail tatiana.itina@univ-st-etienne.fr; phone (+33) 477915829.

Notes

The authors declare no competing financial interest.

ACKNOWLEDGMENTS

We gratefully acknowledge financial support from The "Programme Avenir Lyon-Saint-Etienne", France under PALSE "ERTIGO" project. Computer support was provided by CINES of France through the project c2015085015. We thank Dr. Bévillon for providing DFT-based calculated

DOI: 10.1021/acs.jpcc.5b02084
J. Phys. Chem. C XXXX, XXX, XXX−XXX

temperature-dependent EDOS for gold and Dr. Colombier for his help in manuscript preparation.

REFERENCES

(1) Viñes, F.; Gomes, J. R. B.; Illas, F. Understanding the reactivity of metallic nanoparticles: Beyond the extended surface model for catalysis. *Chem. Soc. Rev.* **2014**, *43*, 4922−4939.
(2) Scholl, J. A.; Koh, A. L.; Dionne, J. A. Quantum plasmon resonances of individual metallic nanoparticles. *Nature* **2012**, *483*, 421−427.
(3) Fedlheim, D. L.; Foss, C. A. *Metal Nanoparticles: Synthesis, Characterization, and Applications*; CRC Press: Boca Raton, FL, 2001.
(4) Zeng, S.; Yu, X.; Law, W.-C; Zhang, Y.; Hu, R.; Dinh, X.-Q.; Ho, H.-P.; Yong, K.-T. Size dependence of Au NP-enhanced surface plasmon resonance based on differential phase measurement. *Sens. Actuators, A* **2013**, *176*, 1128−1133.
(5) Lee, K.; El-Sayed, M. Gold and silver nanoparticles in sensing and imaging: Sensitivity of plasmon response to size, shape, and metal composition. *J. Phys. Chem. B* **2006**, *110*, 19220−19225.
(6) Chang, W.-S.; Ha, J.; Slaughter, L.; Link, S. Plasmonic nanorod absorbers as orientation sensors. *Proc. Natl. Acad. Sci. U.S.A.* **2010**, *107*, 2781−2786.
(7) Anker, J.; Hall, W.; Lyandres, O.; Shah, N.; Zhao, J.; Van Duyne, R. Biosensing with plasmonic nanosensors. *Nat. Mater.* **2008**, *7*, 442−453.
(8) Last, I.; Ron, S.; Heidenreich, A.; Jortner, J. Coulomb explosion of nanodroplets drives the conversion of laser energy to nuclear energy. *High Power Laser Sci. Eng.* **2013**, *1*, 69−73.
(9) Kennedy, L. C.; Bickford, L. R.; Lewinski, N. A.; Coughlin, A. J.; Hu, Y.; Day, E. S.; Drezek, R. A. A. New era for cancer treatment: Gold-nanoparticle-mediated thermal therapies. *Small* **2011**, *7*, 169−183.
(10) Zweiback, J.; Cowan, T.; Hartley, J.; Howell, R.; Wharton, K.; Crane, J.; Yanovsky, V.; Hays, G.; Smith, R.; Ditmire, T. Detailed study of nuclear fusion from femtosecond laser-driven explosions of deuterium clusters. *Phys. Plasmas* **2002**, *9*, 3108−3120.
(11) Letfullin, R.; Joenathan, C.; George, T.; Zharov, V. Laser-induced explosion of gold nanoparticles: Potential role for nano-photothermolysis of cancer. *Nanomedicine* **2006**, *1*, 473−480.
(12) Ashiq, M. G. B.; Saeed, M. A.; Tahir, B. A.; Ibrahim, N.; Nadeem, M. Breast cancer therapy by laser-induced Coulomb explosion of gold nanoparticles. *Chin. J. Cancer Res.* **2013**, *25*, 756−761.
(13) Ashiq, M. G. B.; Saeed, M. A.; Ibrahim, N.; Shahid, M. Laser induced Coulomb explosion of gold nanoparticles: Application of nanophotolysis for breast cancer. *Int. Pulse Laser Appl. Adv. Phys.* **2012**, *2*, 1−3.
(14) Lkhagvadulam, B.; Kim, J. H.; Yoon, I.; Shim, Y. Size-dependent photodynamic activity of gold nanoparticles conjugate of water soluble purpurin-18-N-methyl-D-glucamine. *Biomed. Res. Int.* **2013**, No. 720579.
(15) Chen, N.-T.; Tang, K.-C.; Chung, M.-F.; Cheng, S.-H.; Huang, C.-M. Enhanced plasmonic resonance energy transfer in mesoporous silica-encased gold nanorod for two-photon-activated photodynamic therapy. *Theranostics* **2014**, *4*, 798−807.
(16) Huang, X.; Jain, P. K.; El-Sayed, I. H.; El-Sayed, M. A. Plasmonic photothermal therapy (PPTT) using gold nanoparticles. *Lasers Med. Sci.* **2008**, *23*, 217−228.
(17) Fu, M.; Wang, K.; Long, H.; Yang, G.; Lu, P.; Hetsch, F.; Rogach, A. L. Resonantly enhanced optical nonlinearity in hybrid semiconductor quantum dot−metal nanoparticle structures. *Appl. Phys. Lett.* **2012**, *100*, No. 063117.
(18) Werner, D.; Ueki, T.; Hashimoto, S. Methodological improvement in pulsed laser-induced size reduction of aqueous colloidal gold nanoparticles by applying high pressure. *J. Phys. Chem. C* **2012**, *116*, 5482−5491.
(19) Werner, D.; Furube, A.; Okamoto, T.; Hashimoto, S. Femtosecond laser-induced size reduction of aqueous gold nanoparticles: In situ and pump−probe spectroscopy investigations revealing Coulomb explosion. *J. Phys. Chem. C* **2011**, *115*, 8503−8512.
(20) Itina, T. E. On nanoparticle formation by laser ablation in liquids. *J. Phys. Chem. C* **2011**, *115*, 5044−5048.
(21) Povarnitsyn, M. E.; Levashov, P.; Khishchenko, K.; Itina, T. E. Mechanisms of nanoparticle formation by ultra-short laser ablation of metals in liquid environment. *Phys. Chem. Chem. Phys.* **2013**, *15*, 3108−3114.
(22) Last, I.; Levy, Y.; Jortner, J. Beyond the Rayleigh instability limit for multicharged finite systems: from fission to Coulomb explosion. *Proc. Natl. Acad. Sci. U.S.A.* **2012**, *99*, 9107−9112.
(23) Plech, A.; Kotaidis, V.; Lorenc, M.; Boneberg, J. Femtosecond laser near-field ablation from gold nanoparticles. *Nat. Phys.* **2006**, *2*, 44−47.
(24) Kaganov, M. I.; Lifshits, I. M.; Tanatarov, L. V. Relaxation between electrons and the crystalline lattice. *Sov. Phys. - JETP* **1957**, *4*, 173−178.
(25) Anisimov, S. I.; Kapeliovich, B. L.; Perel'man, T. L. Electron emission from metal surfaces exposed to ultrashort laser pulses. *Sov. Phys. - JETP* **1974**, *39*, 375−377.
(26) Giammanco, F.; Giorgetti, E.; Marsili, P.; Giusti, A. Experimental and theoretical analysis of photofragmentation of Au nanoparticles by picosecond laser radiation. *J. Phys. Chem. C* **2010**, *114*, 3354−3363.
(27) Lin, Z.; Zhigilei, L. V.; Celli, V. Electron-phonon coupling and electron heat capacity of metals under conditions of strong electron-phonon nonequilibrium. *Phys. Rev. B* **2008**, *77*, 075133.
(28) Bévillon, E.; Colombier, J.-P.; Recoules, V.; Stoian, R. Free-electron properties of metals under ultrafast laser-induced electron-phonon nonequilibrium: a first-principles study. *Phys. Rev. B* **2014**, *89*, 115117.
(29) The Engineering ToolBox, http://www.engineeringtoolbox.com (accessed May 18, 2015).
(30) Green, D. W.; Perry, R. H. *Perry's Chemical Engineers' Handbook*, 8th ed.; McGraw-Hill: New York, 2007
(31) Ekici, O.; Harrison, R. K.; Durr, N. J.; Eversole, D. S.; Lee, M.; Ben-Yakar, A. Thermal analysis of gold nanorods heated with femtosecond laser pulses. *J. Phys. D: Appl. Phys.* **2008**, *41*, No. 185501.
(32) Hergert, W.; Wriedt, T. *The Mie Theory: Basics and Applications*; Springer Series in Optical Sciences, Vol. *169*; Springer-Verlag: Berlin and Heidelberg, Germany, 2012
(33) Johnson, P. B.; Christy, R. W. Optical constants of the noble metals. *Phys. Rev. B* **1972**, *16*, 12.
(34) Pyatenko, A.; Yamaguchi, M.; Suzuki, M. Mechanisms of size reduction of colloidal silver and gold nanoparticles irradiated by Nd:YAG laser. *J. Phys. Chem. C* **2009**, *113*, 9078−9085.
(35) Pyatenko, A.; Yamaguchi, M.; Suzuki, M. Synthesis of spherical silver nanoparticles with controllable sizes in aqueous solutions. *J. Phys. Chem. C* **2007**, *111*, 7910−7917.
(36) Egry, I.; Lohoefer, G.; Jacobs, G. Surface tension of liquid metals: Results from measurements on ground and in space. *Phys. Rev. Lett.* **1995**, *75*, 4043.
(37) Gouriet, K.; Sentis, M.; Itina, T. E. Molecular dynamics study of nanoparticle evaporation and condensation in a gas. *J. Phys. Chem. C* **2009**, *113*, 18462−18467.
(38) Hashimoto, S.; Werner, D.; Uwada, T. Studies on the interaction of pulsed lasers with plasmonic gold nanoparticles toward light manipulation, heat management, and nanofabrication. *J. Photochem. Photobiol. C* **2012**, *13*, 28−54.
(39) Plimpton, S. Fast parallel algorithms for short-range molecular dynamics. *J. Comput. Phys.* **1995**, *117*, 1−19.
(40) Schoolcraft, T. A.; Constable, G. S.; Zhigilei, L. V.; Garrison, B. J. Molecular dynamics simulation of the laser disintegration of aerosol particles. *Anal. Chem.* **2000**, *72*, 5143−5150.
(41) Muto, H.; Miyajima, K.; Mafune, F. Mechanism of laser-induced size reduction of gold nanoparticles as studied by single and double laser pulse excitation. *J. Phys. Chem. C* **2008**, *112*, 5810−5815.
(42) Itina, T. E.; Zhigilei, L. V.; Garrison, B. J. Microscopic mechanisms of matrix assisted laser desorption of analyte molecules:

DOI: 10.1021/acs.jpcc.5b02084
J. Phys. Chem. C XXXX, XXX, XXX−XXX

Insights from molecular dynamics simulation. *J. Phys. Chem. B* **2002**, *106*, 303−310.
(43) Itina, T. E.; Zhigilei, L. V.; Garrison, B. J. Matrix-assisted pulsed laser evaporation of polymeric materials: A molecular dynamics study. *Nucl. Instrum. Methods Phys. Res., Sect. B* **2001**, *180*, 238−244.

DOI: 10.1021/acs.jpcc.5b02084
J. Phys. Chem. C XXXX, XXX, XXX−XXX